UDC 539.4

Force Model and Elastic Deformation Analysis of 20-High Sendzimir Mill Rolls

Z. H. Wang,[a,1] Y. L. Lei,[b] Y. H. Feng,[a] and H. F. Hu[a]

[a] Key Laboratory of Metallurgical Equipment and Control of Education Ministry, Wuhan University of Science and Technology, Wuhan, Hubei, China

[b] College of Mechanical and Electronic Information, China University of Geosciences, Wuhan, Hubei, China

[1] zhwang@wust.edu.cn

A 20-high Sendzimir mill is widely used in cold rolling. The deformation of rolls within the roll system as a whole is analyzed without pin-pointing upon each roll and impact on the rolling process. The mechanical model of the work roll, first intermediate roll, second intermediate driven roll, and second intermediate idler roll was proposed and the contact force of each roll was calculated in the rolling process. The finite element model was constructed on the basis of calculation results, the elastic deformation of each roll was analyzed in three rolling passes. It was found that the resultant force of the work roll was the maximum of all rolls, and the maximum elastic deformation of each roll was observed in the second rolling pass; the radial elastic deformation of each roll would influence the plate, its quality, viz. an uneven strip thickness. Each roll is subjected to cyclic stress, so the bending deformation of roll can reduce its service life, producing the fatigue crack.

Keywords: Sendzimir mill, roll system, contact force, elastic deformation.

Introduction. A 20-high Sendzimir mill has a lot of advantages, such as large pass reduction, low energy consumption, and low operating costs. Due to a small diameter, high stiffness, the 20-high mill is widely used in the rolling of cold-rolled stainless steel, electrical steel, ultra-thin steel plates and high-precision strips. The control of strip quality and operational stability is an important issue of current research [1, 2].

Malik and Grandhi [3] predicted the static cross-sectional strip thickness with a new computational method, which simulates the profile and flatness of the strip of improved efficiency and accuracy, it involves a novel combination of the Timoshenko beam finite elements with multiple coupled Winkler elastic beds. Wang et al. [4, 5] constructed a mechanical model for the roll system of a 20-high mill in the rolling process, analyzed the static pressure of the roll system and force conditions in the rolling process. The results demonstrate that the resultant force of the second intermediate driven roll, second intermediate idler roll, intermediate backup roll, and backup roll on both sides is 59.5–62%, 37.7–40.3%, 87.1–88.7%, and 53.9–56.7% of the roll force, respectively. Zhang et al. [6] gave the definition and made calculation of the stability of the roll system of a 20-high mill and listed stability criteria of the force analysis of the roll system. ADAMS was used to simulate the deformation and stability of the roll system, the result shows that the deformation has little effect on the stability of the roll system. Zhang et al. [7] built the three-dimensional elastic finite element model of the roll system of a Sendzimir mill in the roll contact zone by ANSYS, and calculated the complex deformation of the roll system. With the model, the complex elastic deformation and contact stress of the rolls were correctly evaluated and the plate shape control capability of a Sendzimir mill were analyzed.

Yu et al. [8, 9] used the matrix to analyze the rolling process of a Sendzimir mill, which is the contact element method (CEM) with two relative coordinates. Also SMSM (Setup Models for Sendzimir Mill) software was used whereby one can study the strip edge

reduction during rolling. It was found that with an increase in the first intermediate roll taper slope and length and reduction in the shift of the first intermediate roll, the strip edge drop would decrease and in contrast, it would increase with the convexity of the work and second intermediate idler rolls, or with the tensile stress. Li et al. [10] developed the new analytical model for precise prediction of the deflections and radius control. Considering the interactions of the rolls, the stand and the strip workpiece, the numerical method is widely used to solve the theoretical rolling force, the deformation and the inherent force-deflection relationship. In order to assess the accuracy of predicted deflections, a series of profile measurements was performed and to validate the radius control model, various control methods were used in the tests. Liu et al. [11] used the 3D elastic-plastic FEM to simulate the cold strip rolling process in a 4-high mill. The elastic deformation of the rolls, plastic deformation of the strip and the pressure between the work and backup rolls were considered. By way of simulation, the peak value and its location for rolling pressure were analyzed under different conditions. It can determine the effects of bending force in the roll and strip width on the distribution of rolling pressure along the width direction.

Cho et al. [12] proposed the new model, which can be used for multihigh mill to precisely predict the deformed profile, it can also be used in analyzing the deformation of rolls of a 20-high Sendzimir mill under special conditions, such as rigid outer rolls and no-roll shifting. By comparing with the finite element simulation, the prediction accuracy of the new model is proved. Shin et al. [13] proposed the numerical model based on the contact element method. The numerical model considers the relationships between the actuating forces, roll deflections, thickness profiles of the inlet and outlet sides and the strip shape, it was found that the proposed strip shape prediction method based on the CEM can characterize the changes in position of the shape actuators. Zhang et al. [14] investigated and developed the simulation model and software tools, which are used to analyze the strip shape control performance of a 20-high Sendzimir mill, the roll system and deformation of the plate rolling of 20-high Sendzimir mill at a silicon steel factory were simulated and calculated. The results show that the shape control ability of dual ASU is about 2.3 times as much as single ASU. The smooth transition of the cone angle of the conical section of the first intermediate roll can reduce the peak value of the contact pressure between rolls by using the quadratic parabola as the roll shape curve, etc. Wang [15] analyzed the structural improvements of a 20-high Sendzimir mill, which is used for rolling a BA stainless steel plate, in some detail.

A ZR-22BS-42 Sendzimir mill at a silicon steel factory was taken as the object of the study. The mechanical model of the work roll, first intermediate roll, second intermediate driven roll, and second intermediate idler roll was developed. According to the calculation results of the contact force among each roll, the finite element model of each roll was set up, and the effect of the deformation of each roll on the control of profile quality and operational stability of the mill was analyzed. The results are of importance for the design and strength check of matching rolls and rollers of the roll system of the mill [16, 17], the design and optimization of the mill pressure adjustment mechanism and convexity adjustment device. They can also be used for the design and manufacture of a new mill.

1. **Model**.

1.1. ***Roll Structure***. The roll system structure of a 20-high Sendzimir mill is shown in Fig. 1. The rolls of a 20-high Sendzimir mill are mounted symmetrically in eight plug bearings with the frame of a 1-2-3-4 pyramidal arrangement, it consists of 2 work rolls *S* and *T*, 4 first intermediate rolls *O*, *P*, *Q*, and *R*, 6 second intermediate rolls *I*, *J*, *K*, *L*, *M*, and *N*, and 8 backup rolls *A*, *B*, *C*, *D*, *E*, *F*, *G*, and *H*. *I*, *N*, *K*, and *L* on both sides of the mill are the second intermediate driven rolls, the motor power is transferred to the mill through a universal joint shaft. *J* and *H* are the second intermediate idler rolls, each roll rotates due to the friction against each other. The rolling force is applied by the work roll, passing the first

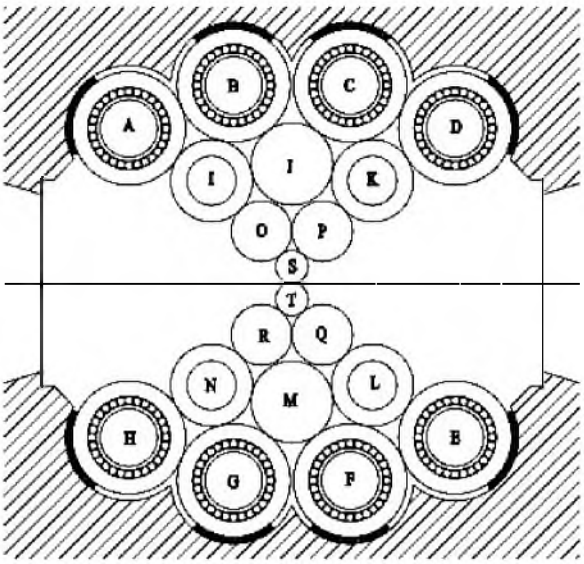

Fig. 1. The roll system structure of a 20-high Sendzimir mill.

intermediate roll, the second intermediate roll to the backup roll, which is a multipoint supported beam structure, and the roll force is evenly radiated over the bracket.

1.2. ***The Work Roll.*** The location of the work roll S and its stress diagram are depicted in Fig. 2. P_{np} is the roll force, a is the roll force arm, ν is the direction angle of the roll force, P_A is the contact force between the work roll S and the first intermediate roll O, α_A and φ_A are the direction angle and geometrical angle of P_A, respectively, P_B is the contact force between the work roll S and the first intermediate roll P, α_B and φ_B are the direction angle and geometrical angle of P_B, respectively, and m_1 is the roll friction arm of the work roll S and the first intermediate rolls O and P.

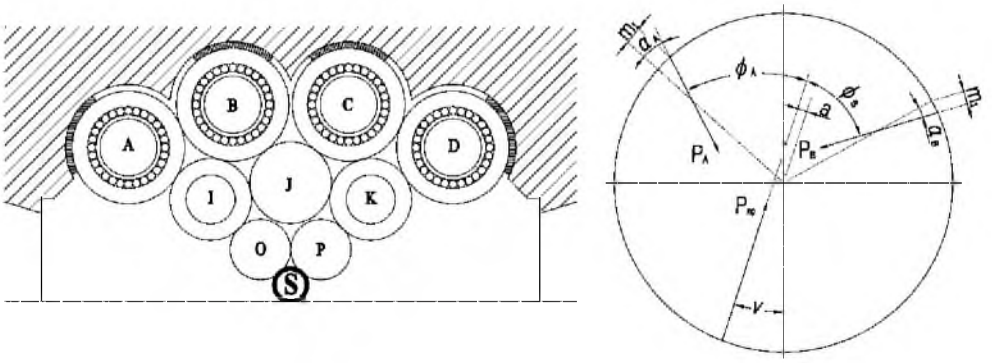

Fig. 2. The work roll S.

The mechanical model of the work roll S is given by:

$$P_A \sin(\varphi_A + \nu - \alpha_A) = P_B \sin(\varphi_B - \nu + \alpha_B), \tag{1}$$

$$P_{np} = P_A \cos(\varphi_A + \nu - \alpha_A) + P_B \cos(\varphi_B - \nu + \alpha_B), \tag{2}$$

$$aP_{np} = P_A (R_S \sin\alpha_A - m_1) + P_B (R_S \sin\alpha_B - m_1). \tag{3}$$

1.3. ***The First Intermediate Roll***. The location of the first intermediate roll P and its stress diagram are presented in Fig. 3. P_E is the contact force between the first intermediate roll P and the second idler roll J, α_E and φ_E are the direction angle and geometrical angle of P_E, respectively, P_F is the contact force between the first intermediate roll P and the second driven roll K, α_F and φ_F are direction angle and geometry angle of P_F, respectively, m_4 is the rolling friction arm of the first intermediate roll P and the second intermediate idler roll J, and m_2 is the rolling friction arm of the first intermediate roll P and the second intermediate idler roll K.

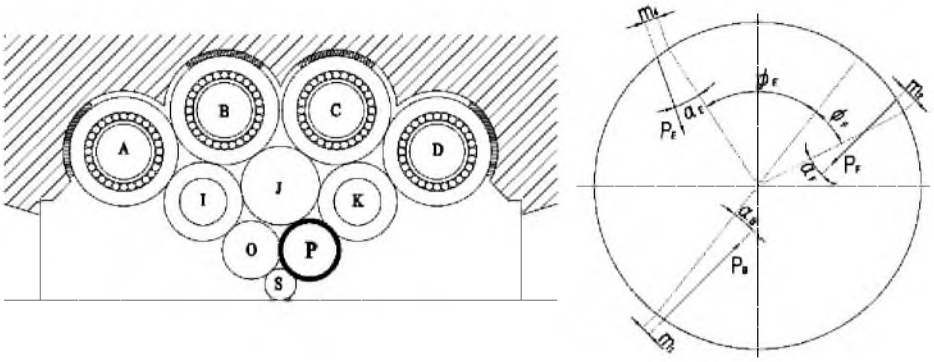

Fig. 3. The first intermediate roll P.

The mechanical model of the first intermediate roll P is shown as follows:

$$P_E \sin(\varphi_E + \alpha_B - \alpha_E) = P_F \sin(\varphi_F - \alpha_B - \alpha_F), \tag{4}$$

$$P_B = P_E \cos(\varphi_E + \alpha_B - \alpha_E) + P_F \cos(\varphi_F - \alpha_B - \alpha_F), \tag{5}$$

$$P_F (R_P \sin\alpha_F - m_2) = P_B (R_P \sin\alpha_B + m_1) + P_E (R_P \sin\alpha_E + m_4). \tag{6}$$

1.4. ***The Second Intermediate Driven Roll***. The location of the second intermediate driven roll K and its stress diagram are illustrated in Fig. 4. P_K is the contact force between the second intermediate driven roll and backup roll C, α_K and φ_K are the direction angle and geometrical angle of P_K, respectively, P_L is the contact force between the second intermediate driven roll K and backup roll D, α_L and φ_L are the direction angle and geometrical angle of P_L, respectively, M_K is the drive torque, m_3 is the rolling friction arm in the second intermediate driven roll K and backup roll A, and m_5 is the rolling friction arm of the second intermediate driven roll K and backup roll C.

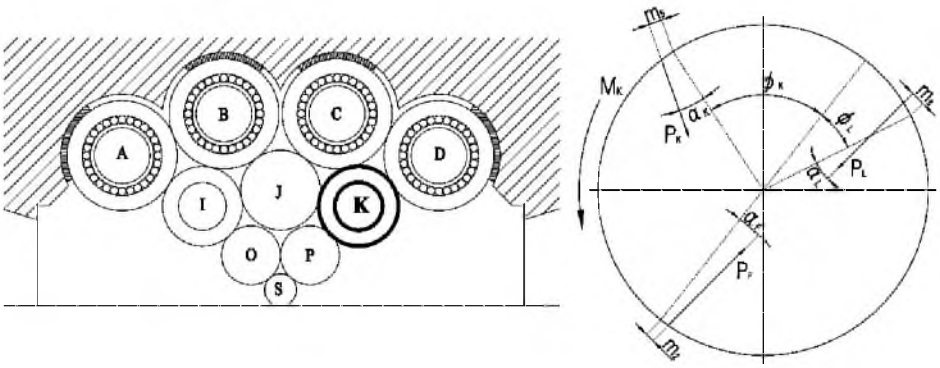

Fig. 4. The second intermediate driven roll K.

The mechanical model of the second driven roll K is expressed as

$$P_K \sin(\varphi_K + \alpha_K - \alpha_F) = P_L \sin(\varphi_L + \alpha_F - \alpha_L), \tag{7}$$

$$P_F = P_K \cos(\varphi_K + \alpha_K - \alpha_F) + P_L \cos(\varphi_L + \alpha_F - \alpha_L), \tag{8}$$

$$M_K = P_F (R_K \sin\alpha_F + m_2) + P_L (R_K \sin\alpha_L + m_3) + P_K \sin(R_K \sin(R_K \sin\alpha_K + m_5). \tag{9}$$

1.5. ***The Second Intermediate Idler Roll***. The location of the second intermediate idler roll J and its force diagram are shown in Fig. 5. P_I is the contact force between the second intermediate idler roll J and backup roll B, α_I and φ_I are the direction angle and geometric angle of P_I, respectively, P_J is the contact force between the second intermediate idler roller J and backup roll C, α_J and φ_J are the directional angle and geometrical angle of P_J, respectively, while v_1 and v_2 are the mechanical model position angles of the second intermediate idler roll J for O and P, respectively.

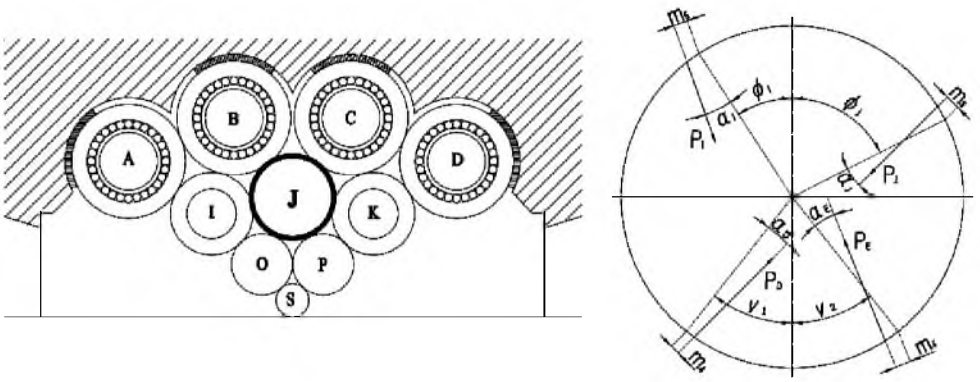

Fig. 5. The second intermediate idler roll J.

The mechanical model of the second intermediate idler roll J is shown as follows:

$$P_I \sin(\varphi_I + \alpha_K + v_3) - P_J \sin(\varphi_J - \alpha_J - v_3) = 0, \tag{10}$$

$$P_{DE} - P_I \cos(\varphi_I + \alpha_I + v_3) = P_J \cos(\varphi_J - \alpha_J - v_3), \tag{11}$$

$$P_D (R_J \sin\alpha_D - m_4) + P_E (R_J \sin\alpha_E - m_4) =$$

$$= P_I (R_J \sin\alpha_I + m_5) + P_J \sin(R_J \sin\alpha_I + m_5), \tag{12}$$

$$P_{DE} = \sqrt{P_D^2 + P_E^2 - 2P_D P_E \cos(180 - v_1 - v_2)}, \tag{13}$$

$$v_3 = v_1 + \alpha_D - \beta_E. \tag{14}$$

2. **Calculation**.

2.1. ***Parameters and Rolling Plans of the Roll System***. For this study, a set of rolling parameters of a ZR-22BS-42 Sendzimir mill at a silicon steel factory was chosen [5]: the mill power is 4000 kW, the base rate is 257 m/min, the maximum rolling force is 6200 kN, the strip width is 1020 mm, the inlet thickness is 2.22 mm, the outlet thickness is 0.75 mm,

and the coil weight is 15 t. The highest speed of the first rolling pass is 450 m/min, second rolling pass is 800 m/min, third rolling pass is 800 m/min. The maximum reduction of the first rolling pass is 34%, second rolling pass is 28.1%. According to the rolling plans, the parameters for each roll are summarized in Table 1, the rolling plan of different rolling passes is given in Table 2.

T a b l e 1

Rolling Parameters of a ZR-22BS-42 Sendizimir Mill

Roll type	Nominal diameter (mm)	Minimum roll diameter (mm)	Maximum roll diameter (mm)	Hardness (HRC)
Work roll	63.5	58	73.5	60–62
First intermediate roll	102.0	96	105.0	58–58
Second intermediate roll	173.0	170	173.0	58–60
Backup roll	300.0	297	300.0	68–74

T a b l e 2

Rolling Plan for a ZR-22BS-42 Sendzimir Mill

Rolling pass	Rolling force (kN)	Inlet tension (MPa)	Outlet tension (MPa)	Inlet thickness (mm)	Outlet thickness (mm)	Yield strength (MPa)	Rolling speed (m/min)
1	3390	15	161	2.22	1.645	68.9	450
2	3720	112	197	1.645	1.043	92.3	630
3	3670	157	218	1.043	0.75	103.9	705

2.2. ***Calculation Process and Results***. Since stress relationships for the roll system of a 20-high Sendzimir mill is rather compound, more accurate calculation results can be obtained with computer. The iteration method is applied to each rolling parameter, assuming that the roll system is in the initial position, taking the rolling parameters and rolling plans as the initial conditions, and setting the calculation accuracy at $x = 0.001$ [18, 19], the results can be processed with MATLAB software. According to the flow chart, the magnitude and direction angle of the contact force between rolls in different rolling processes are given in Tables 3 and 4, the calculation results of the rolling friction arm m are shown in Table 5.

T a b l e 3

Contact Forces between Rolls in Different Rolling Processes

Rolling pass	P_A, kN	P_B, kN	P_D, kN	P_E, kN	P_F, kN	P_I, kN	P_J, kN	P_K, kN	P_L, kN
1	2254.5	2130.55	1026.4	460.3	1380.8	751.2	1150.9	503.3	1275.7
2	2542.5	2274.30	1220.4	460.2	1492.5	753.2	1252.6	511.2	1285.3
3	2510.3	2241.40	1220.4	460.5	1490.7	750.5	1253.8	511.2	1288.1

Table 4

Direction Angles of the Contact Force between Rolls in Different Rolling Processes

Rolling pass	α_A, deg	α_B, deg	α_D, deg	α_E, deg	α_F, deg	α_I, deg	α_J, deg	α_K, deg	α_L, deg
1	2.331	2.331	0.253	0.253	5.643	0.112	0.112	0.112	5.643
2	2.675	2.675	0.25	0.25	6.182	0.112	0.112	0.112	6.23
3	2.573	2.573	0.25	0.25	6.082	0.112	0.112	0.112	6.18

Table 5

Rolling Friction Arms in Different Rolling Passes of the Rolling Process on a ZR-22BS-42 Sendzimir Mill

Rolling pass	m_1, mm	m_2, mm	m_3, mm	m_4, mm	m_5, mm
1	0.1238	0.1390	0.2002	0.0958	0.1418
2	0.1293	0.1463	0.2128	0.0768	0.1266
3	0.1291	0.1449	0.2106	0.1001	0.1462

3. Analysis and Discussion.

3.1. *Finite Element Models.*

3.1.1. *Simplified Model.* According to the calculation results of the magnitude, direction angle, and related parameters of the contact force in each roll, the finite element model for each roll was constructed. In order to simplify calculations with the finite element model, speed up solving appropriately, each roll model was simplified as follows: the structure of every roll is assumed to be a beam structure. Considering the lateral motion of each roll in the rolling process, the length of the line load of each roll is equal to the length of the axial contact of each roll. All transition fillets and chamferings of the core shaft of each roll are ignored. The simplified models of the work roll, first intermediate roll, second intermediate driven roll, and second intermediate idler roll were used with HYPERWORKS software.

3.1.2. *Meshing.* The hexahedral grid was used in meshing each roll. After meshing the work roll *S*, 198,018 nodes and 187,090 units were received. After meshing the first intermediate roll *P*, 308,534 nodes and 294,510 units were obtained. After meshing the second intermediate driven roll *K*, 559,143 nodes and 539,858 units were formed. After meshing the second intermediate idler roll *J*, 601,007 nodes and 581,217 units were produced.

3.1.3. *Constraint and Load.* The roll material is 9Cr2MoV steel, the Young modulus is 210 GPa, Poisson's ratio is 0.3. Four constraints were established in two end faces of the work roll *S*, first intermediate roll *P*, and second intermediate idler roll *J*, except for the motion and rotation along the *z* axis direction. Because the second intermediate driven roll *K* is connected to the motor through a universal joint shaft, its axial shift should be limited, so five constraints, except for the rotation of *z* axis were established. Stresses are applied to each roll, and their calculation results are presented in Tables 3 and 4, and the finite element models for the rolls are shown in Fig. 6.

3.2. *Results and Discussion.*

3.2.1. *The Work Roll.* The problem is solved with a Hyperworks 12 Model. The elastic deformation in three rolling passes of the work roll *S* is increased 30 times (Fig. 7). The resultant force and elastic deformation in the first rolling pass are the smallest, while the largest ones are in the second rolling pass. The maximum elastic deformation is 6.939 mm

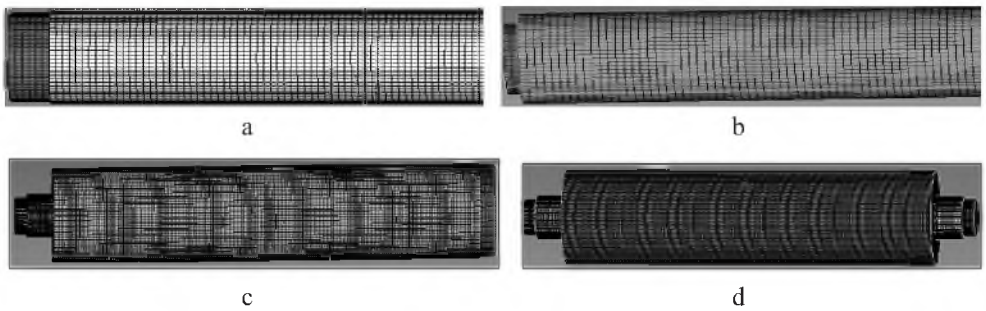

Fig. 6. Finite element models for the rolls: (a) work roll *S*; (b) first intermediate roll *P*; (c) second intermediate driven roll *K*; (d) second intermediate idler roll *J*.

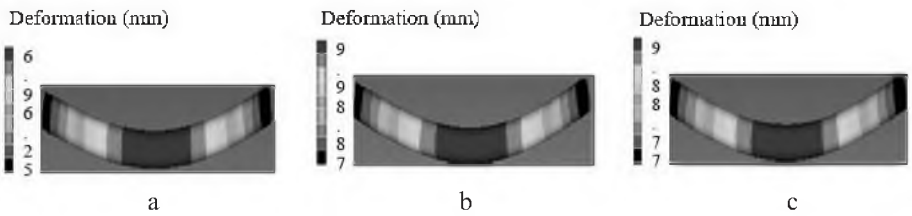

Fig. 7. The work roll *S*. (Here and Figs. 8–10: (a) first rolling pass; (b) second rolling pass; (c) third rolling pass.)

in the first rolling pass, 9.905 mm in the second rolling pass and 9.784 mm in the third rolling pass. Since the work roll accepts the rolling force and the largest resultant force directly, the elastic deformation of the work roll is the largest of all rolls. Two work rolls are in direct contact with the plate, accepting the main rolling force. They have the smallest diameter but largest rolling force in the roll system, so their deflection is the largest. The radial deflection is making the strip thickness uneven, with thin mid-portion and thick edges. Therefore, in order to minimize the bending deformation of the work roll, its stability can be enhanced by improving the flexibility and the rigidity does by changing the structure, making it difficult for the bending deformation to arise in the rolling process.

3.2.2. *The First Intermediate Roll*. The elastic deformation in three rolling passes of the first intermediate roll *P* is increased 30 times (Fig. 8). The maximum elastic deformation is 2.026 mm in the first rolling pass, 4.331 mm in the second rolling pass, and 3.909 mm in the third rolling pass. The force of the first intermediate roll is smaller than that of the work roll, and the rolling force falls greatly as a result of passing through the work roll, so the deformation of the first intermediate roll is smaller than that of the work one. The elastic deformation of the first intermediate roll can be transferred to the rolled plate through the work roll. The axial roll adjustment mechanism of the first intermediate roll can prevent the thickness uneveness, four first intermediate rolls are flat, one end of each roll has a conical surface (conical roll of the two first intermediate rolls at the top are located on the operation side of the mill and conical roll of the two first intermediate rolls at the bottom are located on the transmission side), and the other end is flat, the first top intermediate roll and the first bottom intermediate roll adjust the length of the coincident parallel part by axial motion in its relative or opposite direction, namely cooperate with the convexity adjustment mechanism to complete the shape adjustment. Horizontal adjustment is used to eliminate the strip edge waviness that is caused by the bending deformation of the work roll in the rolling process, through the axial roll shape adjustment system, the coincident parallel length of the two pairs of the first intermediate rolls get changed, consequently, the shape of the strip edge was improved. Therefore, through improving the

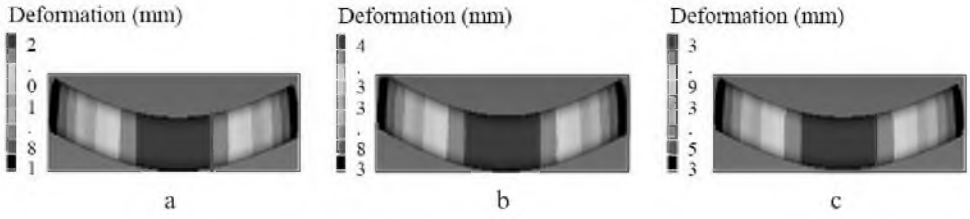

Fig. 8. The first intermediate roll *P*.

accuracy of the adjustment system of the first intermediate roll, the roll strip shape can be controlled in rolling, before and after rolling.

3.2.3. *The Second Intermediate Driven Roll*. The elastic deformation in three rolling passes of the second intermediate driven roll *K* is increased 350 times (Fig. 9). The maximum elastic deformation is 0.443 mm in the first rolling pass, 0.699 mm in the second rolling pass, and 0.686 mm in the third one. As compared to the first intermediate roll, the diameter of the second intermediate driven roll is larger and the rolling force is greatly reduced by passing through the work roll and the first intermediate roll, so the elastic deformation of the second intermediate driven roll is smaller than that of the work and first ones. The elastic deformation of the second intermediate driven roll will be transferred to the rolled plate through the first intermediate roll and work roll. Moreover, four second intermediate driven rolls are arranged on both sides of the rolling mill, they are connected to the motor through a universal joint shaft, which is the source of the rolling mill power, so the deformation of the second intermediate driven roll will affect the stability and accuracy of the transmission, lead to the vibration of the rolling mill. It may lead to the direct failure of rolling. So the control of the bending deformation is also of great importance.

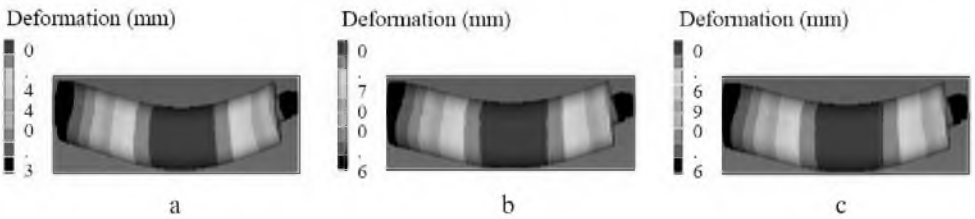

Fig. 9. The second intermediate driven roll *K*.

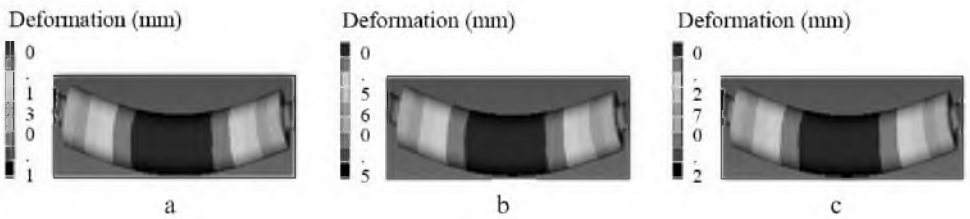

Fig. 10. The second intermediate idler roll *J*.

3.2.4. *The Second Intermediate Idler Roll*. The elastic deformation in three rolling passes of the second intermediate idler roll *J* is increased 400 times (Fig. 10). The maximum elastic deformation is 0.130 mm in the first rolling pass, 0.564 mm in the second rolling pass, and 0.274 mm in the third rolling pass. The force of the second intermediate

driven roll on both sides is larger than that of the second intermediate idler roll, so the elastic deformation of the second intermediate idler roll is smaller than that of the driven roll. Its elastic deformation will also affect the rolling plate thickness through the first intermediate roll and work roll. Two second intermediate idler rolls are symmetrically arranged in the middle of the rolling mill, the second intermediate driven roll and second intermediate idler roll are contacting directly, the driven roll conveys power to the idler roll through friction force, and the idler roll also transmits power to the other roll by friction force. Since the second intermediate idler roll is the first medium of power transmission and in order to prevent the distortion of power in the process of transmission, it is also very important to control the deformation of the second intermediate idler roll. The reduction in hardness of the intermediate roll or increase in hardness of the work roll, i.e., the improvement of the hardness difference between the middle roll and work roll, can contribute to the quality of the plate and prevent from transferring roll body defects to the plate.

Conclusions

1. The work roll is the first to accept the largest resultant force, the next ones are the first intermediate roll and second intermediate driven roll, while the second intermediate idler roll accepts the smallest force. The maximum force and elastic deformation of the rolls are observed in the second rolling pass.

2. The roll rotation during the rolling process can induce their radial deflection, with their offsetting relative to each other. Their bending deformation would affect the plate quality, causing the waviness of strip edges.

3. Due to the symmetry of the roll system, 1/2 or 1/4 of the rolls is often taken as the object in parallel studies, but stresses are not actually distributed symmetrically. Inaccuracies in arrangement and coordination, differences in manufacturing and heat treatment lead to the differences in forces, so that forces of the rolls O and P are 2144.57 and 2180.03 kN, respectively.

This study is not restricted to a 20-high mill, it also creates the theoretical basis for the design and improvement of multiroll mills with other roll numbers.

1. E. Brusa and L. Lemma, "Numerical and experimental analysis of the dynamic effects in compact cluster mills for cold rolling," *J. Mater. Process. Tech.*, **209**, No. 5, 2436–2445 (2009).
2. L. S. Wang, Q. Yang, and A. R. He, "Improvement of prediction model for work roll thermal contour in hot strip mill," *J. Centr. South Univ. Technol.*, **17**, No. 6, 1251–1257 (2010).
3. A. S. Malik and R. V. Grandhi, "A computational method to predict strip profile in rolling mills," *J. Mater. Process. Tech.*, **206**, No. 1, 263–274 (2008).
4. Z. H. Wang, Q. J. Gao, and C. Yan, "Calculation and analysis of the force in roll system of 20-high Sendzimir mill," *J. Iron Steel Res. Int.*, **20**, No. 9, 33–39 (2013).
5. Z. H. Wang, Y. C. Yan, and Y. B. Zhang, "Analyzing exerted forces on a roll system of 20-high Sendzimir mill in rolling process," *J. Huazhong Univ. Sci. Technol.*, **41**, No. 2, 17–21 (2013).
6. Q. D. Zhang, L. J. Zhang, and M. Yu, "Analysis on the stability of roll system of 20-h Sendzimir mill," *Heavy Machinery*, No. 6, 19–25 (2007).
7. L. J. Zhang, Q. D. Zhang, and M. Yu, "Analysis on shape control behavior of 20-h Sendzimir mill by finite element method," *Metall. Equip.*, No. 1, 40–43 (2008).

8. H. L. Yu, X. H. Liu, and G. T. Lee, "Numerical analysis of strip edge drop for Sendzimir mill," *J. Mater. Process. Tech.*, **208**, No. 1, 42–52 (2008).
9. H. L. Yu, X. H. Liu, and G. T. Lee, "Numerical analysis of roll deflection for Sendzimir mill," *J. Manuf. Sci. Eng.*, **130**, No. 1, 011016-1–011016-7 (2008).
10. Z. J. Li, H. Yang, and H. W. Li, "A new model for precision control of the radius in in-plane roll-bending of strip considering rolls and stand deflections," *J. Mater. Process. Tech.*, **211**, No. 12, 2072–2084 (2011).
11. X. H. Liu, S. Xu, and S. Q. Li, "FEM analysis of rolling pressure along strip width in cold rolling process," *J. Iron Steel Res. Int.*, **14**, No. 5, 22–26 (2007).
12. J. H. Cho and S. M. Hwang, "A new model for the prediction of roll deformation in a 20-high Sendzimir mill," *J. Manuf. Sci. Eng.*, **136**, No. 1, 011004 (2014).
13. J. Shin, S. Han, and J. Kim, "Development and experimental evaluation of strip shape prediction model for Sendzimir rolling mills," *J. Iron Steel Res. Int.*, **20**, No. 12, 25–32 (2013).
14. Q. Zhang, C. Dai, and J. Wen, "Simulation and analysis on shape control behavior of 20-h Sendzimir mill," *Steel Rolling*, **30**, No. 3, 1–6 (2013).
15. Q. J. Wang, "Technology design of 20-roller Sendzimir cold rolling mill for BA-stainless steel," *Industrial Heating*, **42**, No. 3, 56–58 (2013).
16. Z. H. Bai, K. Wang, and Y. J. Wang, "Inner roll shape optimization design technology of VC mill," *China Mech. Eng.*, **24**, No. 22, 3096–3100 (2013).
17. W. Zhang, Y. Q. Wang, and M. H. Sun, "Research on automatic gauge control model of strip mills," *China Mech. Eng.*, **19**, No. 1, 95–98 (2008).
18. C. J. Pan, *20-High Sendzimir Mill and High Precise Cold Rolling Production*, Metallurgical Industry Press, Beijing (2003).
19. H. Q. Huang, *Steel Rolling Machine*, Metallurgical Industry Press, Beijing (1980).

Received 30. 08. 2016